Free Convection Heat Transfer From Spheroids

G. D. Raithby
Thermal Engineering Group, Department of Mechanical Engineering, University of Waterloo, Waterloo, Ontario, Canada
Mem. ASME

A. Pollard
Department of Mechanical Engineering, Imperial College of Science and Technology, London, England

K. T. G. Hollands
Mem. ASME

M. M. Yovanovich
Mem. ASME

Thermal Engineering Group, Department of Mechanical Engineering, University of Waterloo, Waterloo, Ontario, Canada

Measurements of the heat transfer by free convection from isothermal spheroids to air are reported. The range of Rayleigh number, Ra, covered was sufficiently large that both thick boundary layer effects (at low Ra) and turbulence (at high Ra) affect the heat transfer. Data are reported for one prolate spheroid and two oblate spheroids. The results of an approximate method of analysis, which accounts for both thick boundary layers and turbulence, are also given. These are compared to the present measurements, and to earlier measurements for spheres. Excellent agreement with experiment is found. Correlation equations, from which average heat transfer rates can be calculated, are also given. These are thought to be valid at all Rayleigh numbers over a large range of eccentricity.

1 Introduction

Recent years have seen a rapid intensification of research related to the measurement, prediction, and understanding of heat transfer by free convection. For external free convection, measurements and predictions have focussed on problems where the flow is two-dimensional (e.g., vertical plates and cylinders, tilted plates, horizontal circular cylinders) or axisymmetric (e.g., spheres). References [1–10][1] list some of the important contributions to these problems from the analysis side.

The solutions in references [1–10] are obtained from simplified equations of motion which contain the boundary-layer approximations and which ignore curvature effects (the equations are written in local Cartesian coordinates). Also, no account has been taken of turbulent heat transfer from part or all of the surface.

Langmuir [11] recognized the importance of accounting for curvature effects and a few solutions, including at least some of these effects, have been obtained [12–16]. Reference [16] also makes allowance for turbulent heat transfer. It was shown in [16] that, for two-dimensional bodies, there is often *no* range in Rayleigh number for which solutions, ignoring curvature effects and turbulence, are in agreement with experiment. In this paper we extend this study to some axisymmetric bodies (spheroids). The organization of the presentation is as follows.

First, measurements are reported for isothermal spheroids of various eccentricities immersed in quiescent air. Previous measurements have been apparently restricted to spheres [17–21(*a*)].

Second, these measurements are compared with three analyses; the first of these neglects curvature and turbulence effects, the second corrects for curvature effects but neglects turbulence, the third accounts for both. The method of prediction is that proposed by Raithby and Hollands [16, 22]. By comparing experiment and these results of analyses it is possible: (*a*) to make a statement about the range of Rayleigh number over which adequate predictions of an *average* Nusselt number can be expected from analyses based on local Cartesian coordinates, and (*b*) to evaluate the success of the Raithby-Hollands method for accounting for turbulence and curvature effects.

Third, based on the analytical results, correlation equations are then obtained from which the average heat transfer from spheroids of moderate eccentricity can be calculated.

A separate note in this issue of the journal [22(*a*)] extends the analysis to the case of prolate spheroids with high eccentricity; these resemble vertical needles, tapered from the center toward both ends.

2 Experiment

Measurements of heat transfer by free convection from oblate and prolate spheroids of moderate eccentricity ($C/B = 0.5$), and from one

[1] Numbers in brackets designate References at end of paper.

Contributed by the Heat Transfer Division for publication in the JOURNAL OF HEAT TRANSFER. Manuscript received by the Heat Transfer Division March 3, 1976. Paper No. 76-HT-BBB.

Table 1 Constants f_1 and f_2

C/B	Prolate Spheroid f_1	Prolate Spheroid f_2	Prolate Spheroid $2\hat{}f_2^{\sharp}/f_1$	Oblate Spheroid f_1	Oblate Spheroid f_2	Oblate Spheroid $2\hat{}f_2^{\sharp}/f_1$
1.000	2.000	1.683	0.878	2.000	1.683	0.878
0.900	1.935	1.653	0.896	1.868	1.601	0.906
0.800	1.873	1.624	0.913	1.739	1.518	0.935
0.700	1.814	1.596	0.931	1.615	1.435	0.966
0.600	1.759	1.570	0.948	1.494	1.352	0.997
0.500	1.709	1.545	0.964	1.380	1.269	1.030
0.400	1.665	1.524	0.980	1.274	1.187	1.062
0.300	1.627	1.506	0.993	1.177	1.108	1.091
0.200	1.598	1.491	1.005	1.094	1.033	1.114
0.100	1.578	1.481	1.012	1.030	0.969	1.128
0.050	1.573	1.479	1.014	1.009	0.945	1.129
0.010	1.571	1.478	1.015	1.001	--	--
0.005	1.571	1.478	1.015	1.000	--	--
0.001	$\approx \pi/2$	1.478	1.015	1.000	--	--

Table 2 Values of f_3 (equation (5)) and n (equation (6))

(C/B)	f_3 Oblate Spheroid	f_3 Prolate Spheroid	n Oblate Spheroid	n Prolate Spheroid
1.00	0.73	0.73	6	6
0.80	0.79	0.73	5	6
0.60	0.87	0.72	5	6
0.50	0.93	0.71	4	6
0.40	0.99	0.71	3	6
0.20	1.20	0.71	2.5	6
0.10	1.44	0.71	2.5	-
0.05	1.73	0.71	-	-
0.01	--	0.71	-	-

oblate spheroid of large eccentricity ($C/B = 0.1$) to air are reported. Notation, cross-sectional drawings, and pertinent data on these spheroids are presented in Fig. 1.

The objective of the experiments was to measure *average* Nusselt numbers over a large Rayleigh-number range. This range was achieved by locating the spheroids in a pressure vessel (a cylinder 38.5 cm in diameter and 150 cm long) and performing the measurements at various pressure levels (as. for example, in [23, 24]) between 0.028 and 2.35 bar. The wall of the pressure vessel was maintained at a uniform temperature by water cooling. Its temperature, required for radiation corrections, and the air temperature far removed from the spheroid-location, were both measured using shielded thermocouples. The air pressure was measured using a U-tube manometer to an overall accuracy of ±0.0005 bar. Measurements showed that there was no appreciable thermal stratification of the air during the experiments.

Large spheroids were desired in order to obtain a significant turbulent heat transfer, but their size was limited by the additional requirement that enclosure effects [25] be unimportant; the compromise dimensions appear in Fig. 1. Isothermal-surface boundary conditions were achieved by manufacturing the spheroids from a high thermal conductivity material (Aluminum 6061-T6) and by keeping a low internal resistance to heat flow. The contours of the spheroids were accurately machined and their surfaces finely polished.

Two thermocouple junctions were imbedded at different locations in each spheroid and the leads buried in shallow grooves in the surface which conducted the wires to the rear stagnation region. A small heater (5 mm in diameter for the $C/B = 0.5$ spheroids and 3 mm for the $C/B = 0.1$ spheroid) was also imbedded through the rear stagnation region. A high thermal conductivity cement was used to fill the grooves and the space around the heater. Current was fed to the heater through two very fine bare wires (as small as 0.25 mm dia); some of the experiments were repeated using lead wires of different diameter and material. The mass of each spheroid was accurately determined by weighing; the mass of the heater, thermocouple wires, and cement amounted, in the worst case, to 0.4 percent of the total spheroid mass. Prior to testing, the appropriate spheroid was suspended in the center of the pressure cylinder from 0.3 mm nylon leads, and its axis of symmetry precisely aligned with the vertical direction. The cold junctions of the spheroid thermocouples were radiation shielded and located on the center line of the pressure vessel, one on each side of, and 50 cm removed from, the spheroid; the voltage output of these was a direct measure of the spheroid-to-air temperature difference.

The heat transfer from the spheroid was determined by measuring its transient temperature decay from an initially heated state. Nor-

Nomenclature[2]

A_s = surface area of spheroid, equation (B.6)
B = dimension of spheroid along its major axis
C = dimension of spheroid along its minor axis
C_ℓ = "universal" function of Pr for laminar flow $C_\ell = 0.50/[1 + (0.49/\mathrm{Pr})^{9/16}]^{4/9}$
$\hat{C}_\ell = 4C_\ell/3$
C_t = "universal" function of Pr for turbulent flow. $C_t = [0.14\ \mathrm{Pr}^{0.084}, 0.15]^*$, where $[A, B]^*$ = minimum of A and B
f_1, f_2 = definite integrals defined in Appendix B. Numerical values are given in Table 1
f_3: defined by equation (5)
k: thermal conductivity
ℓ: see Table B.1
m: see Table B.1
n: exponent in correlation equation, numerical values appear in Table 2
$\overline{\mathrm{Nu}}_B$ = average Nusselt number for spheroid based on the length B (measured, or predicted from analysis which includes thick-layer and turbulence effects)
$(\overline{\mathrm{Nu}}_B)_{\ell t}$ = predicted average Nusselt number based on laminar, thin-layer analysis (Appendix B)
$(\overline{\mathrm{Nu}}_B)_\ell$ = predicted average Nusselt number based on laminar analysis, where corrections for thick-layer effects have been made (Appendix B)
$(\overline{\mathrm{Nu}}_B)_{\mathrm{cond}}$ = Nusselt number in the conduction limit (equation (3))
$(\overline{\mathrm{Nu}}_B)_t$ = average Nusselt number from analysis in which turbulent heat transfer is presumed everywhere on the surface, and Ra_B is very large
Pr = Prandtl number calculated at temperature $(T_s + T_\infty)/2$
Ra_B = Rayleigh number based on ΔT and B
S = one-half the perimeter of body in flow direction
T_s = temperature of spheroid
T_∞ = temperature of ambient air far from spheroid
$\Delta T = T_s - T_\infty$
(η, θ, Ψ) = spheroidal coordinates (see Appendix B)

[2] Where symbols have been used only once, they are defined immediately after their appearance in the text, and are not repeated here.

mally, the surface temperature was elevated to 44°C above ambient and it was allowed to cool to 36°C before measurements were recorded. The rate of change of its temperature with time was determined by accurately measuring the time for the temperature difference to decrease by 0.6°C. The voltage output of the thermocouple determining the temperature difference was measured using a Leads and Northrup K-5 potentiometer (±0.005 percent of reading or ±0.1 μV, i.e., ±0.006°C). After making this measurement, the pressure, air temperature and wall temperature in the cylinder were noted. The Rayleigh number was calculated using the mean temperature difference over the measurement period, and evaluating all air properties at the average film temperature; all properties were calculated from equations by Hilsenrath [26]. The total rate of heat loss was determined from the measurements and a knowledge of the spheroid mass and specific heat. To calculate the heat transfer by free convection, upon which the Nusselt number is based, required corrections for radiation and conduction via the lead wires.

The heat transfer by radiation was determined using the measured temperatures, the surface area of the spheroid, and its emissivity. The total normal emissivity of a sample of the aluminum, with a similar surface finish, was measured on a Gier-Dunkle DB100 Reflectometer and this was converted to the hemispherical emissivity shown in Fig. 1 (see Eckert and Drake [27]). The heat loss by conduction along the nylon support wires, the thermocouple lead wires, and the heater lead wires was calculated by the method outlined in Appendix A. All of the lead losses were normally small, but at low pressures the heat transfer along the heater leads climbed to 16 percent of the heat loss by free convection. The calculated total heat loss via the leads and by radiation were subtracted from the total heat loss, and the Nusselt number calculated.

Five such measurements were repeated in rapid succession and an average Nusselt number and Rayleigh number were formed. A total of 78 of 85 recorded sets of data are reported. The unreported sets are those in which experimental conditions varied during the course of taking the measurements, or the total heat loss via the leads exceed 13 percent of the heat loss by free convection.

Experimental Results. For all the test conditions used, the Prandtl number was about 0.71 (actually $0.709 < Pr < 0.711$). For the prolate spheroid with $C/B = 0.5$, the $\bar{N}u_B$ versus Ra_B results are plotted in the lower part of Fig. 2. The data show very little scatter and measurements for different heater-lead wires are entirely consistent. The solid curve drawn through the data is an analytical result which will be described later.

The upper part of Fig. 2 shows some experimental results by Elenbaas [18] and Mathers, et al. [19] for spheres ($C/B = 1.0$) and correlation equations based on the experimental results of Kyte, et al. [17], Tsubouchi and Sato [20], Yuge [21], and Amato and Tien [21a].

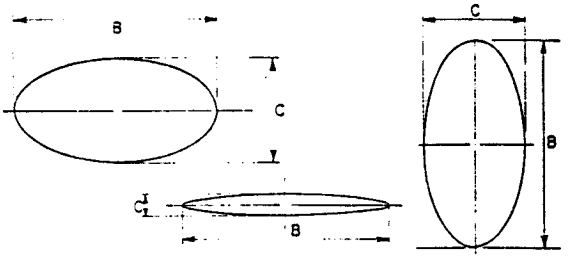

	C/B = 0.5 OBLATE SPHEROID (SIDE VIEW)	C/B = 0.1 OBLATE SPHEROID (SIDE VIEW)	C/B = 0.5 PROLATE SPHEROID (SIDE VIEW)
C (mm)	39.2	8.00	40.0
B (mm)	78.6	80.0	77.1
MASS (kg)	0.341	0.0734	0.174
EMISSIVITY	0.056	0.056	0.056
SPECIFIC HEAT (kJ/kg C)	0.96	0.96	0.96

Fig. 1 Top and side views of spheroids, showing dimensions and other data

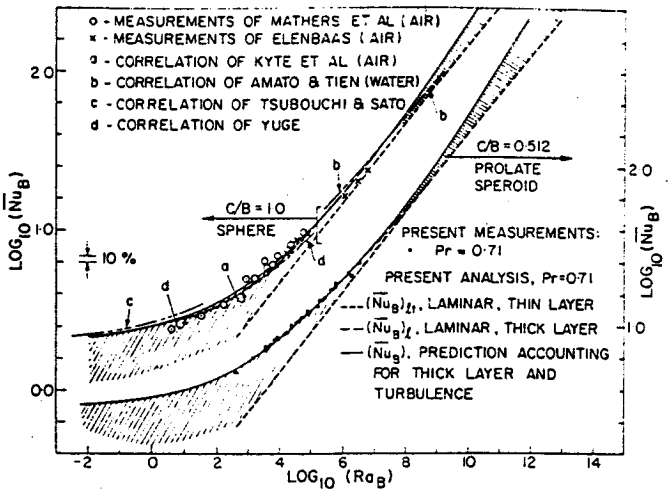

Fig. 2 Data, results of analysis, and correlation equations for prolate spheroid (lower) and sphere (upper)

Other curves are the result of the present analysis.

The data for the two oblate spheroids are plotted in Fig. 3. There is again little scatter in the measurements and no systematic differences between results obtained using different heater leads. The solid curves are the results of the analysis, which is now described.

3 Analysis

The foregoing measurements are now compared with analysis, keeping in mind the concerns expressed in the Introduction over the effects of curvature and turbulence on the average heat transfer. The first section in the following presents a simple analysis which neglects curvature and turbulence effects; the second corrects this result for curvature effects, and the third accounts for both curvature *and*

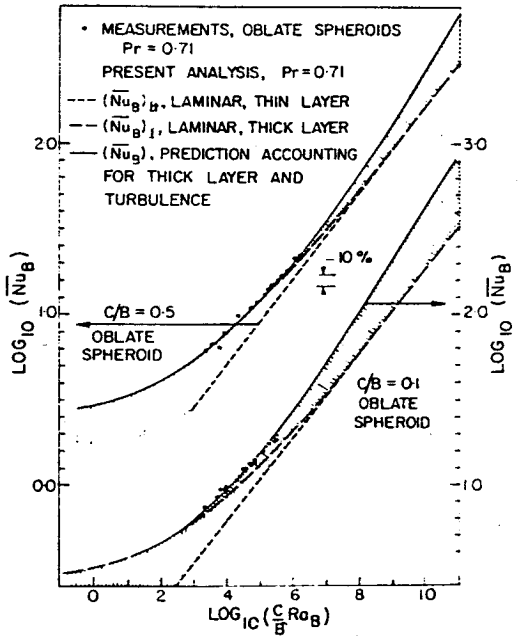

Fig. 3 Present data for two oblate spheroids, and the results of analysis

turbulence. Building up the analysis in this step-by-step way permits a direct insight into the relative importance of these effects.

Laminar, Thin-Layer Results. The term "thin-layer" [16] is associated with laminar boundary-layer analyses in which local Cartesian coordinates are used in expressing the conservation constraints. Thus, the general solutions for bodies of arbitrary contour [9, 10], and many of the other solutions to free convection problems, fall into this category. The results presented here are obtained by a direct application of the thin-layer solution of Raithby and Hollands [22]. Although this solution is approximate, it has been shown to be in good agreement with other thin-layer analyses for vertical plates and horizontal elliptic cylinders [16] and spheres [22] with uniform temperature boundary conditions. The form of the solution is correct, it is accurate to about 1 percent for isothermal surfaces for $\mathrm{Pr} \gtrsim 0.5$, and the evaluation of the solution is very easy.

An abbreviated account of the application of this solution to the spheroid problem is given in Appendix B. The final result for the average Nusselt number is

$$(\overline{\mathrm{Nu}}_B)_{\ell t} = \frac{\bar{h}B}{k} = \frac{2^{1/4} f_2^{3/4}}{f_1} \bar{C}_\ell \left(\frac{m}{B}\mathrm{Ra}_B\right)^{1/4} \tag{1}$$

where f_1 and f_2 are definite integrals whose values are given in Table 1, where $\bar{C}_\ell$ is a "universal" function of Prandtl number (see Nomenclature), and $m = B$ for prolate spheroids and $m = C$ for oblate spheroids. The subscript ℓt on the Nusselt number is a reminder that this is the laminar, thin-layer prediction.

Equation (1) is plotted in Figs. 2 and 3. The agreement is closest for spheres, followed by the prolate spheroid, the $C/B = 0.5$ and $C/B = 0.1$ oblate spheroids, respectively. For the $C/B = 0.1$ oblate spheroid, the data point nearest to the thin-layer prediction is about 32 percent high, with discrepancies at other Rayleigh numbers becoming (rapidly) larger. It is quite clear that the thin-layer analysis is considerably in error for all the geometries tested.

Correction for Thick-Layer Effects. As already suggested, writing the underlying equations in local Cartesian coordinates neglects important curvature or "thick-layer" effects when the boundary layers are not "thin." A detailed discussion of this, and a method of making a first-order correction to the thin-layer results to account for it, has been given previously [16]. Briefly described, the method consists of dividing the spheroid surface into a large number of segments and using the thin-layer solution to *estimate* the conduction thickness at each location. From the local surface shape (curvature), the local resistance to heat transfer from each segment can be estimated, and therefore one can correct the heat flux. The local heat flux is estimated in this way for each segment of the surface and the results numerically integrated to yield the total heat transfer (and, therefore, the average Nusselt number). The curves labeled $(\overline{\mathrm{Nu}}_B)_\ell$ in Figs. 2 and 3 have been obtained in this way, and the region between this curve and the thin-layer result has been cross-hatched to emphasize the magnitude of the correction. The correction is very significant over a large Rayleigh number range, diminishing only at high Rayleigh numbers where the boundary layers are thin.

It should be kept clearly in mind that:

(*a*) no account has yet been made for turbulence; and

(*b*) the Nusselt numbers, corrected for thick-layer effects, have been obtained by numerical integration so that these can no longer be *directly* evaluated from a closed-form solution.

Comparing measurements and these $(\overline{\mathrm{Nu}}_B)_\ell$ predictions, one finds excellent agreement for spheres and the prolate spheroid in Fig. 2, at least over the Rayleigh number range for which data are available. In Fig. 3, there is good agreement between these predictions and the data at lower Rayleigh numbers for the $C/B = 0.5$ oblate spheroid, but this gradually worsens at higher Ra_B. For the $C/B = 0.1$ oblate spheroid, the correction has improved the agreement but the data lie consistently above the prediction.

The main reason for the disagreement which remains is postulated to be the existence of turbulent heat transfer. This seems consistent with the above observations, for the areas first affected by turbulence (for an increasing Rayleigh number) would be the rear portions of the oblate spheroids. This is particularly true of the $C/B = 0.1$ spheroid where the rear surface is very nearly horizontal.

Allowance for Turbulent Heat Transfer. The procedure for accounting for turbulent heat transfer is described *very* briefly in Appendix B. The details are recorded elsewhere [16, 22].

The predictions, accounting for both turbulence and thick-layer effects, are depicted by the solid lines in Figs. 2 and 3. The curves are labeled $\overline{\mathrm{Nu}}_B$. The area between the $(\overline{\mathrm{Nu}}_B)_\ell$ results and these final predictions is cross-hatched to permit an immediate appreciation of the Rayleigh number range where turbulence is important, and the magnitude of this effect on the total heat transfer.

A comparison with the present data in these two figures indicates that these "final" predictions of the Nusselt number are in excellent agreement with the data. Most agree to within 5 percent (68 out of a total of 78 data points); the maximum difference is about 15 percent.

While the agreement between analysis and measurement is highly satisfactory, it is necessary to point out that the validation of the analysis at high Rayleigh numbers is incomplete. Measurements at higher Rayleigh numbers would be needed to complete the comparison. Also the reader is reminded that the analysis for heat transfer from the lower surface of the oblate spheroid is invalid in the limit as $C/B \to 0$, but this may not be a serious deficiency for predictions of $\overline{\mathrm{Nu}}_B$ since the heat transfer is dominated by turbulence on the top surface.

Data are available for spheres over a large range of Rayleigh number. Fig. 2 shows that the predictions for this geometry are also in excellent agreement with the measurements and correlations of Kyte, et al. [17], Elenbass [18], Mathers, et al. [19], Tsubouchi, et al. [20], and Yuge [21] (all for air), and in somewhat poorer agreement with the Amato-Tien [21(*a*)] correlation for water (partly because the Prandtl number is different, and partly because their equation does not fit their data well at the highest Rayleigh numbers). The agreement of the analysis with the present and earlier measurements for such a wide range of geometries lends strong support to the present method of analysis, and, therefore, to the other predictions for which experimental data are not yet available.

Graphs of $\overline{\mathrm{Nu}}_B$ for spheroids of other eccentricities are given in Figs. 4 (prolate) and 5 (oblate). From Fig. 4 it is seen that almost the same asymptotic relation between $\overline{\mathrm{Nu}}_B$ and Ra_B is approached for *all* eccentricities at high Rayleigh numbers. At the other extreme, the conduction limit, the $\overline{\mathrm{Nu}}_B$ value is sensitive to C/B, particularly for the larger eccentricities. If the curves were replotted with $(C/B)\,\mathrm{Ra}_B$ as the independent variable [22(*a*)], all the curves for small C/B would be brought together at small Rayleigh numbers.

For oblate spheroids (Fig. 5), using $(C/B)\,\mathrm{Ra}_B$ as the independent variable brings the high eccentricity curves together at low Rayleigh

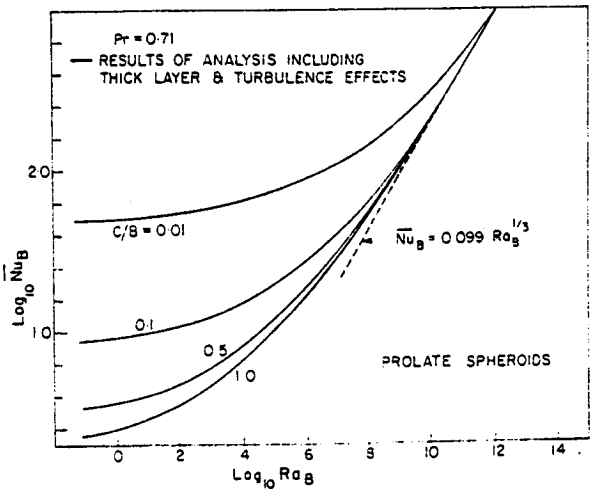

Fig. 4 Predictions for prolate spheroids

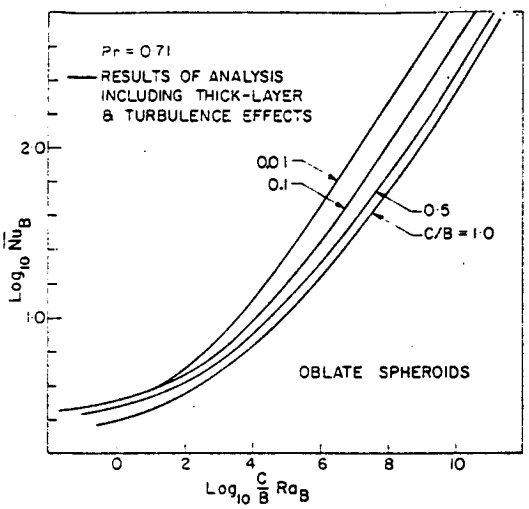

Fig. 5 Predictions for oblate spheroids

numbers, but distinctly different asymptotes are obtained for high Rayleigh numbers. If the independent variable were changed to Ra_B, the turbulent-heat transfer asymptotes would not be greatly different for different eccentricities; however, the curves would cross one another at intermediate Rayleigh numbers and a confusing graph would emerge.

4 Correlation Equations for Moderate Eccentricities

The "final" results of the analysis, plotted in the figures, have been obtained by carrying out the numerical integrations indicated in Appendix B. While this is neither a laborious task (the nonoptimized computer program in Fortran had about 120 statements), nor an expensive one (in terms of computing time), it would be more convenient if the results could be expressed in the form of equations. Equations have been obtained which are accurate for a wide range of eccentricities for both oblate and prolate spheroids; these are described in this section. It should be kept clearly in mind that the equations represent an *empirical fit* to the results of the analysis.

The equation should be constructed such that it has the correct asymptotes for small and large Ra_B, yet also fits the analytical results accurately at intermediate values. Since it is not immediately obvious what form this equation should take, the complexity of the problem was reduced by seeking first asymptotic equations which would be valid for laminar and turbulent heat transfer, respectively. These equations were then combined to give the desired result.

Evaluation of $(\overline{Nu}_B)_\ell$. First, for the laminar problem, the evaluation of the equations in Appendix B was carried out with the turbulent heat transfer "turned off" (i.e., laminar heat transfer at all locations on the surface). The output was values of laminar Nusselt number, $(\overline{Nu}_B)_\ell$, for various C/B and Ra_B; some of these Nusselt numbers have already been plotted in Figs. 2 and 3. For all eccentricities for oblate spheroids and for prolate spheroids for $C/B \gtrsim 0.2$, it was found that these results were very closely fit by an equation of the form

$$(\overline{Nu}_B)_\ell = (\overline{Nu}_B)_{cond} + (\overline{Nu}_B)_{\ell t} \tag{2}$$

where $(\overline{Nu}_B)_{cond}$ is the value of $\bar{N}u_B$ in the conduction limit and $(\overline{Nu}_B)_{\ell t}$ is the Nusselt number from the laminar, thin-layer analysis, [equation (1)]. The error in approximating $(\overline{Nu}_B)_\ell$ by this equation is normally less than 1 percent. A maximum error of 2 percent occurs for the prolate spheroid for $C/B = 0.2$ (and 10 percent if the equation were to be used for $C/B = 0.1$).

Equations for $(\bar{N}u_B)_{cond}$ can be obtained directly from the analysis in Appendix B (equation (B-12)). For the prolate and oblate spheroids, respectively, one finds

$$(\overline{Nu}_B)_{cond} = \frac{4\sqrt{1-(C/B)^2}}{f_1} \cdot \frac{-1}{(C/B)\ln\tanh(\eta_i/2)} \quad \text{(for prolate)} \tag{3a}$$

$$(\overline{Nu}_B)_{cond} = \frac{4\sqrt{1-(C/B)^2}}{f_1} \cdot \frac{1}{(\pi/2) - \tan^{-1}(\sinh \eta_i)} \quad \text{(for oblate)} \tag{3b}$$

where f_1 is given in Table 1 and, by definition,

$$\eta_i = 0.5 \ln |[1 + (C/B)]/[1 - (C/B)]| \tag{4}$$

Evaluation of $(\overline{Nu}_B)_t$. Now an equation is sought which is valid at asymptotically high Ra_B when the heat transfer is turbulent at (essentially) all locations on the surface. The corresponding Nusselt number is designated $(\bar{N}u_B)_t$. The analysis suggests that this is proportional to $Ra_B^{1/3}$ for any C/B value. To keep the same independent variables as in the laminar equations, the following equation was used

$$(\overline{Nu}_B)_t = f_3 C_t \left(\frac{m}{B} Ra_B\right)^{1/3} \tag{5}$$

Values of f_3, obtained by rerunning the analysis at a high Ra_B with the laminar heat transfer "turned off," are tabulated in Table 2.

Final Correlation Equations. The foregoing equations for laminar and turbulent heat transfer respectively were combined according to the Churchill-Usagi [28] formula to give the following equation for $\overline{Nu}_B$

$$(\overline{Nu}_B)^n = (\overline{Nu}_B)_\ell{}^n + (\overline{Nu}_B)_t{}^n \tag{6a}$$

where n is a constant chosen to give best agreement between equation (6) and direct calculations of $\bar{N}u_B$. The final equation, therefore, becomes

$$(\overline{Nu}_B)^n = \left[(\overline{Nu}_B)_{cond} + \left(\frac{2^{1/4} f_2^{3/4}}{f_1}\right) \bar{C}_\ell \left(\frac{m}{B} Ra_B\right)^{1/4}\right]^n + \left[C_t f_3 \left(\frac{m}{B} Ra_B\right)^{1/3}\right]^n \tag{6b}$$

where n and f_3 are given in Table 2, f_1 and f_2 in Table 1, $m = B$ and C for prolate and oblate spheroids, respectively, $(\overline{Nu}_B)_{cond}$ is given by equations (3), and $\bar{C}_\ell$ and C_t are Prandtl-number-dependent coefficients listed in the Nomenclature. Equation (6b) has been found to fit the results of the analysis to within about 5 percent.

5 Summary

1 Measurements of the average Nusselt number for free convection heat transfer from one prolate, and two oblate, isothermal, spheroids to quiescent, air at uniform temperature have been reported.

2 The results of an anysis, accounting for both thick-layer (or curvature) effects and turbulent heat transfer has been presented. Excellent agreement with experiment was found; but of perhaps greater significance than the agreement itself, an appreciation of the importance of curvature and turbulence effects was gained.

3 Correlation equations were presented which are valid for a wide range of eccentricity and for all Rayleigh numbers.

Acknowledgments

The work was supported through Operating Grants from the National Research Council of Canada.

We gratefully acknowledge the assistance of Mr. V. A. Wehrle at the Communications Research Centre, Department of Communications, Ottawa, for performing the reported emissivity measurements for aluminum on their Gier-Dunkle Reflectometer. Our thanks also to Prof. D. French and Mr. J. Minnema for their assistance in machining the prolate spheroid.

References

1 Schmidt, E., and Beckmann, W., "Das Temperatur—und Geschwindijkeitsfeld vor einer Warme algebenden senkrechten Platte bei naturlicher Konvection," *Techn. Mechan. und Thermodynamik*, Vol. 11, 1930, pp. 391–406.

2 Ostrach, S., see Bird, R., Stewart, W. E., Lightfoot, E. N., *Transport*

Phenomena, Wiley, New York, 1960.
3 Sparrow, E. M., and J. L. Gregg, "Laminar Free Convection From a Vertical Plate With Uniform Heat Flux," TRANS. ASME, Vol. 78, 1956, pp. 435–440.
4 Braun, W. H., Ostrach, S., and Heighway, J. E., "Free-Convection Similarity Flows About Two-Dimensional and Axisymmetric Bodies With Closed Lower Ends," *International Journal of Heat and Mass Transfer*, Vol. 2, 1961, pp. 121–135.
5 Chiang, T., and Kaye, J., "On Laminar Free Convection From a Horizontal Cylinder," *Proceedings of 4th National Congress of Applied Mechanics*, 1962, pp. 1213–1219.
6 Chiang, T., Ossin, A., and Tien, C. L., "Laminar Heat Transfer From a Sphere," JOURNAL OF HEAT TRANSFER, TRANS., ASME, Series C, Vol. 96, 1964, pp. 537–542.
7 Koh, J. C., "Laminar Free Convection From a Horizontal Cylinder With Prescribed Surface Heat Flux," *International Journal of Heat and Mass Transfer*, Vol. 7, 1969, pp. 811–823.
8 Koh, J. C. Y., and Price, J. F., "Laminar Free Convection From a Non-isothermal Cylinder," JOURNAL OF HEAT TRANSFER, TRANS., ASME, Series C, Vol. 78, 1956, pp. 237–242.
9 Saville, D. A., and Churchill, S. W., "Laminar Free Convection in Boundary Layers Near Horizontal Cylinders and Vertical Axisymmetric Bodies," *Journal of Fluid Mechanics*, Vol. 29, 1967, pp. 391–399.
10 Lin, F. N., and Chao, B. T., "Laminar Free Convection over Two-Dimensional and Axisymmetric Bodies of Arbitrary Contour," JOURNAL OF HEAT TRANSFER, TRANS., ASME, Series C, Vol. 96, 1974, pp. 435–442.
11 Langmuir, I., "Convection and Conduction of Heat in Gases," *Physical Review* Vol. 34, 1912, pp. 401–422.
12 Sparrow, E. M., and Gregg, J. L., "Laminar-Free-Convection Heat Transfer from the Outer Surface of a Vertical Circular Cylinder," TRANS. ASME, 1956, pp. 1823–1829.
13 Minkowycz, W. J., and Sparrow, E. M., "Local Non-similar Solutions for Natural Convection on a Vertical Cylinder," JOURNAL OF HEAT TRANSFER, TRANS., ASME, Series C, Vol. 96, 1974, pp. 178–183.
14 Peterka, J. A., Richardson, P. D., "Natural Convection From a Horizontal Cylinder at Moderate Grashof Numbers," *International Journal of Heat and Mass Transfer*, Vol. 12, 1969, pp. 749–752.
15 Hieber, C. A., "Natural Convection Around Semi-Infinite Vertical Plate: Higher Order Effects," *International Journal of Heat and Mass Transfer* Vol. 17, 1974, pp. 785–791.
16 Raithby, G. D., and Hollands, K. G. T., "Laminar and Turbulent Free Convection from Elliptic Cylinders, with a Vertical Plate and Horizontal Circular Cylinder as Special Cases," JOURNAL OF HEAT TRANSFER, TRANS. ASME, Series C, Vol. 98, 1976, pp. 72–80.
17 Kyte, J. R., Madden, A. J., Piret, E. L., "Natural Convection Heat Transfer at Reduced Pressure," *Chemical Engineering Progress* Vol. 49, 1953, pp. 653–662.
18 Elenbaas, W., "The Dissipation of Heat by Free Convection of Spheres and Horizontal Cylinders," *Physica*, Vol. 9, No. 3, 1942, pp. 285–296.
19 Mathers, W. G., Madden, A. J., and Piret, E. L., "Simultaneous Heat and Mass Transfer in Free Convection," *Fluid Mechanics in Chemical Engineering* Vol. 49, 1957, pp. 961–968.
20 Tsubouchi, T., Sato, S., "Heat Transfer From Fine Wires and Particles by Natural Convection," *Chemical Engineering Progress Symposium Series 30*, Vol. 56, pp. 269–284.
21 Yuge, T., "Experiments on Heat Transfer From Spheres Including Combined Natural and Forced Convection," JOURNAL OF HEAT TRANSFER TRANS., ASME, Vol. 82, 1960, pp. 214–220.
21(a) Amato, W. S., and Tien, C., "Free Convection Heat Transfer From Isothermal Spheres in Water," *International Journal of Heat and Mass Transfer*, Vol. 15, 1972, pp. 327–339.
22 Raithby, G. D., and Hollands, K. G. T., "A General Method of Obtaining Approximate Solutions to Laminar and Turbulent Free Convection Problems," *Advances in Heat Transfer*, Academic Press, 1974; see also *International Journal Heat Mass Transfer* Vol. 17, 1974, pp. 1620–1622.
22(a) Raithby, G. D., and Hollands, K. G. T., "Free Convection Heat Transfer From Vertical Needles," to be published in the JOURNAL OF HEAT TRANSFER, TRANS., ASME.
23 Saunders, O. A., "The Effect of Pressure on Natural Convection in Air," *Proc. Roy. Soc.*, London, Series A, Vol. 157, 1936, pp. 278–291.
24 Thompson, H. A., and Sogin, H. H., "Experiments on the Onset of Thermal Convection in Horizontal Layers of Gases," *Journal Fluid Mechanics* Vol. 24, 1966, pp. 451–479.
25 Powe, R. E., "Bounding Effects on the Heat Loss by Free Convection From Spheres and Cylinders," JOURNAL OF HEAT TRANSFER, TRANS., ASME, Series C, Vol. 96, 1974, pp. 558–560.
26 Hilsenrath, J., et al., "Tables of Thermal Properties of Gases," *U.S. Dept. of Commerce Circular* 564, 1955.
27 Eckert, E. R. G., Drake, R. M., *Heat and Mass Transfer*, McGraw-Hill, New York, 1959.
28 Churchill, S. W., and Usagi, R., "A General Expression for the Correlation of Rates of Transfer and Other Phenomena," *AIChE Journal*, Vol. 18, 1972, pp. 1121–1128.
29 Yovanovich, M. M., "A General Expression for Predicting Conduction Shape Factors, Progress in Astronautics and Aeronautics," *Thermophysics and Spacecraft Thermal Control*, Vol. 35, 1974, pp. 265–291.
30 Fujii, T., Takeuchi, M., Fujii, M., Suzaki, K., and Uehara, H., "Experiments on Natural Convection Heat Transfer From the Outer Surface of a Vertical Cylinder to Liquids," *International Journal of Heat and Mass Transfer*, Vol. 13, 1970, pp. 753–787.
31 Yovanovich, M. M., *Advanced Heat Conduction*, Hemisphere Publishing Corp., Washington, D. C., 1976.

APPENDIX A

Conduction Losses Along Lead Wires

Heat flows from the spheroids along the lead wires by conduction, transferring heat from its surface by radiation and either from or to its surface by convection. The local temperature of the air surrounding the wires changes along their length because they are immersed in the wake of the spheroid. This temperature distribution can be calculated fairly accurately using some reasonable equation based on the conduction thickness, Δ_t. (e.g., equation of Fujii, et al. [30]). A new free convection solution, accounting for both wall and surrounding temperature variations, was derived along the lines of reference [22] to obtain the convective component of the heat transfer from the wire surfaces. An expression for radiative exchange with the surroundings was also obtained. The total loss along the lead was calculated by subdividing the wire into a large number of segments and guessing a longitudinal distribution of temperature. From this guessed distribution the heat transfer by free convection and radiation was computed for each segment and an improved longitudinal distribution was obtained by a finite-difference solution of the heat conduction equation for the wire. The process was repeated until a converged solution was obtained.

APPENDIX B

Details of Heat Transfer Analysis

The Coordinate System and Nomenclature. The application of the general solution of Raithby and Hollands [22] is briefly outlined in this section. This requires converting to, and working in, spheroidal coordinate systems. These coordinates are depicted in Fig. B.1. To avoid giving a separate treatment for each spheroid, several new symbols are introduced and their definitions given in Table B.1.

The spheroids shown in Fig. B.1 are generated by choosing a value of $\eta = \eta_i$ in the coordinate transformation

$$x = a\, g(\eta) \sin\theta \cos\psi,\ y = a\, g(\eta) \sin\theta \sin\psi,\ z = a\, h(\eta) \cos\theta \quad \text{(B.1)}$$

and where θ runs from 0 to π, and ψ from 0 to 2π. a is just a scaling factor with dimensions of length. Curves of constant θ and constant η are, respectively, hyperboloids and ellipsoids. The differential distance in the η, θ, and ψ directions are, respectively, $\sqrt{g_\eta}d_\eta$, $\sqrt{g_\theta}d_\theta$, and $\sqrt{g_\psi}d_\psi$, where the metric coefficients g_η, g_θ and g_ψ have been given

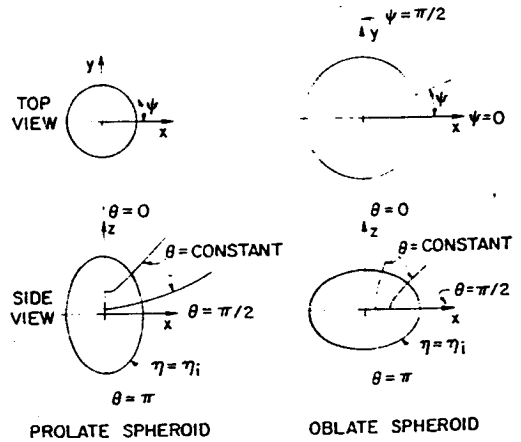

Fig. B.1 Schematic of spheroids showing spheroid coordinate systems

Table B.1 Definition of variables used in Appendix B

Symbol	Prolate spheroid	Oblate spheroid
ℓ	C	B
m	B	C
R	$\ln[\tanh(\eta_0/2)/\tanh(\eta_i/2)]$	$\tan^{-1}(\sinh\eta_0) - \tan^{-1}(\sinh\eta_i)$
S^*	$(\sinh^2\eta + \sin^2\theta)^{1/2}$	$(\cosh^2\eta - \sin^2\theta)^{1/2}$
$g(\eta)$	$\sinh\eta$	$\cosh\eta$
$h(\eta)$	$\cosh\eta$	$\sinh\eta$

by Yovanovich [31] as

$$g_\eta = g_\theta = a^2 S^{*2}; \quad g_\psi = a^2 \sinh^2\eta \sin^2\theta \tag{B.2}$$

Focussing attention on the η_i spheroid in Fig. B.1, from equation (B.1)

$$B = 2a\cosh\eta_i; \; C = 2a\sinh\eta_i; \; r = \sqrt{x^2+y^2} = (\ell/2)\sin\theta \tag{B.3}$$

Fixing the dimensions B and C fixes the scaling factor a and the value of η_i since, by equation (B.3)

$$a = \sqrt{(B/2)^2 - (C/2)^2}; \quad \eta_i = 0.5\ln[(B+C)/(B-C)] \tag{B.4}$$

The differential length, ds_θ, along the surface in the direction of increasing θ on the spheroid is

$$ds = (\sqrt{g_\theta})_{\eta=\eta_i} d\theta = (B/2)[(m/B)^2\sin^2\theta + (\ell/B)^2\cos^2\theta]^{1/2} d\theta = (B/2)\chi(\theta, C/B)d\theta \tag{B.5}$$

Equation (B.5) serves also as a definition for the function χ.

The surface area of the surface, A_s, is given by

$$A_s = \int_0^{2\pi}\int_0^{\pi} (\sqrt{g_{\theta\theta}g_{\psi}})_{\eta=\eta_i} d\theta d\psi = (B\ell/4) \cdot \int_0^{\pi} \sin\theta\,\chi(\theta, C/B)d\theta = (\pi B\ell/2)f_1 \tag{B.6}$$

The integration can be carried out analytically and the resulting equation for f_1 evaluated. Numerical values of f_1 are given in Table 1 in the text.

These equations are now used in evaluating the free-convection heat transfer from the spheroids.

Thin-Layer Analysis. The general solution for the average Nusselt number is given by [22]

$$(\bar{\mathrm{Nu}}_S)_{\ell t} = \bar{C}_\ell \mathrm{Ra}_S^{1/4}\left[\frac{1}{S}\int_0^S \left(r^4\frac{g_s}{g}\right)^{1/3} ds\right]^{3/4} \Big/ \left[\frac{1}{S}\int_0^S r\,ds\right] \tag{B.7}$$

where g_s is the component of g acting along the surface.

Converting from the local Cartesian coordinate s to the spheroid coordinate θ results in equation (1) in which

$$f_2 = \int_0^{\pi} \sin^{5/3}\theta\,\chi^{2/3}\,d\theta \tag{B.8}$$

Numerical values of f_2 are tabulated in Table 1.

Thick-Layer Correction. The local conduction-layer thickness at location s on the surface is [22]

$$\Delta_\ell = s\left[\frac{1}{s}\int_0^s \left(r^4\frac{g_s}{g}\right)^{1/3} ds\right]^{1/4} \Big/ \left[C_\ell \mathrm{Ra}_s^{1/4}\left(r\frac{g_s}{g}\right)^{1/3}\right] \tag{B.9}$$

Converting from s to the spheroid coordinate θ

$$\Delta_\ell = \frac{B}{2^{1/4}C_\ell((m/B)\mathrm{Ra}_B)^{1/4}} \cdot \frac{\chi^{1/3}}{\sin^{2/3}\theta} \cdot \left[\int_0^\theta \sin^{5/3}\theta\,\chi^{2/3}d\theta\right]^{1/4} \tag{B.10}$$

The local value of η_0 a distance Δ_ℓ away from the η_i surface along a curve of constant θ (i.e., normal to the surface) is given by

$$\Delta_\ell(\theta) = a\int_{\eta_i}^{\eta_0} S^*(\eta,\theta)d\eta \tag{B.11}$$

where S^* is defined in Table B.1. The one-dimensional local resistance to heat transfer by conduction between the two spheroids η_i and η_0 at this location θ has been given by Yovanovich [29]. This is used to estimate the local heat transfer. These local values are integrated over the surface to yield the total heat transfer. Converted to an average Nusselt number, one finds

$$(\bar{\mathrm{Nu}}_B)_\ell = \frac{2\sqrt{1-(C/B)^2}}{(\ell/B)f_1}\int_0^{\pi}\frac{\sin\theta}{R(\eta_0(\theta),\eta_i)}d\theta \tag{B.12}$$

where R is given in Table B.1.

$(\bar{\mathrm{Nu}}_B)_\ell$ is the Nusselt number for laminar heat transfer, corrected to account for thick-layer effects. A numerical integration of (B.12) is required. This is easily done by dividing the surface into a large number of intervals of width $\Delta\theta$. The value of Δ_ℓ at the center of each interval is found from equation (B.10). With Δ_ℓ known, equation (B.11) is used to find η_0 at the corresponding locations; again, this must be done numerically. These values are substituted into the expression for R and the integration in (B.12) is performed to obtain the final result.

Accounting for Turbulence. According to the proposed equation for turbulent heat transfer [16], the local conduction-layer thickness is

$$\Delta_t = B/(C_t A(\phi)\mathrm{Ra}_B^{1/3}) \cdot \tag{B.13}$$

where C_t is a "universal" function of Prandtl number (see Nomenclature) and $A(\phi)$ depends on the local surface angle, ϕ, from the vertical. ϕ is related to the spheroid coordinate θ by

$$\phi = \sin^{-1}\{-(C/B)\cos\theta/\chi(C/B,\theta)\} \tag{B.14}$$

From these, the local Nusselt number can be found. The criterion for transition and the application of the analysis follows [16, 22].